Lab Notes

Editors
Thomas M. Moses | Shane F. McClure

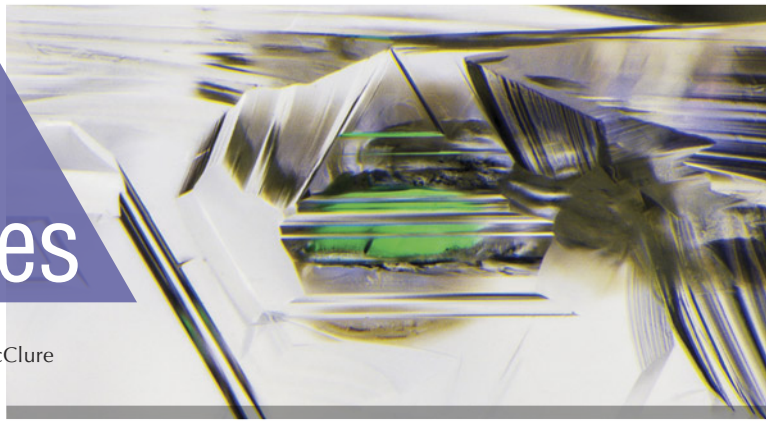

Four-Rayed Star CHRYSOBERYL

GIA's Tokyo laboratory recently received a brownish green cabochon set in a white metal ring with numerous near-colorless marquise brilliants and tapered baguettes (figure 1). The stone measured approximately 12.21 × 9.20 × 8.17 mm. Standard gemological testing showed weak green and yellow pleochroism and a spot refractive index reading of 1.75, as well as a strong diagnostic iron-related 444 nm band observed with a handheld spectroscope. These properties were consistent with chrysoberyl. At first glance the cabochon seemed to display chatoyancy, which would make this a cat's-eye chrysoberyl. However, there was not just a single band of reflected light but two bands intersecting at a 90° angle, so the phenomenon was actually four-rayed asterism.

Chatoyancy is usually created by light reflecting off of parallel needles or tube-like inclusions in a cabochon-cut gemstone. Microscopic observation revealed two sets of inclusions. One consisted of dense minute particles aligned in one direction producing a thick band of reflected light (oriented diagonally in figure 2). The other set was composed of needles oriented along the same direction as the thick band of light. These needles created a second band of reflected light perpendicular to the orientation of the needles. Together, these reflected bands of light resulted in the unique combination of two intersecting cat's-eyes.

Figure 1. Chrysoberyl showing two bands of reflective light displaying four-rayed asterism.

Figure 2. In the star chrysoberyl, short needles and dense minute particles were perpendicular to each other. The particles reflect light and caused the thick band's orientation (seen diagonally here). Field of view 3.7 mm.

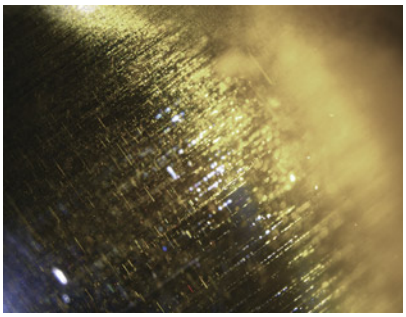

Four-rayed stars are common in diopside, garnet, and spinel. But they are very rare in chrysoberyl, which makes this stone notable.

Yuxiao Li and Yusuke Katsurada

A Closer Look at Internal Etch Channels in DIAMOND

The Carlsbad laboratory recently received a 1.02 ct cushion-cut Fancy Deep brownish yellowish orange diamond (figure 3). The yellowish color of this type Ib/IaA diamond is mainly attributed to single substitutional nitrogen atoms in the diamond lattice. In addition to the presence of multiple pinpoint inclusions, the diamond contained a bundle of internal etch channels extending from a single irregular-shaped opening on the girdle (figures 3 and 4).

Narrow etch channels are rarely observed in gem diamonds. Etch chan-

Figure 3. A 1.02 ct Fancy Deep brownish yellowish orange diamond with subsurface etch channels (upper right).

Editors' note: All items were written by staff members of GIA laboratories.

Gems & Gemology, Vol. 58, No. 4, pp. 474–482.

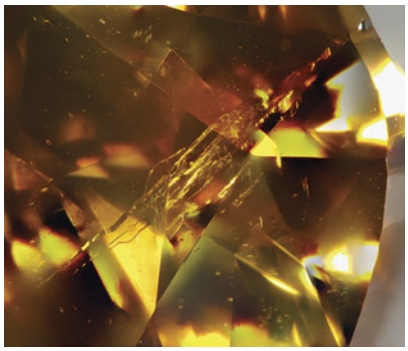

Figure 4. A bundle of internal etch channels extending from a single opening on the girdle. Field of view 2.44 mm.

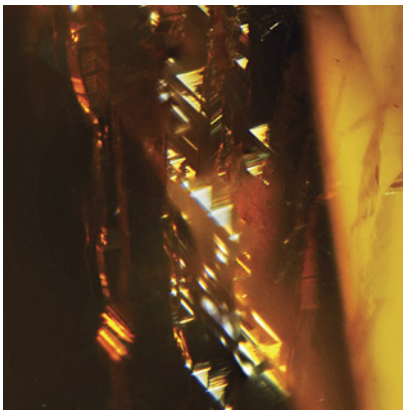

Figure 6. Trigons visible in a subsurface diamond etch channel. Field of view 1.00 mm.

nels can form due to dissolution of the diamond crystal by fluids/melts in the mantle, or during eruption to the surface (T. Lu et al., "Observation of etch channels in several natural diamonds," *Diamond and Related Materials*, Vol. 10, No. 1, 2001, pp. 68–75; J.W. Harris et al., "Morphology of monocrystalline diamond and its inclusions," *Reviews in Mineralogy and Geochemistry*, Vol. 88, No. 1, 2022, pp. 119–166). Defects in the diamond structure such as lattice dislocations are local areas of structural weakness, which are more susceptible to etching. In this diamond, multiple narrow etch channels originate from a single surface opening (figure 5), reflecting selective diamond dissolution as fluids permeated through the stone.

An intriguing feature observed along the walls of the internal etch channels consisted of multiple triangular etch pits known as trigons (figure 6). Trigons are one of the most common features found on the surfaces of rough diamonds, with various sizes, depths, and shapes (e.g., flat- or point-bottomed, attributed to etching by oxidizing fluids/melts; Harris et al., 2022). When present on diamond surfaces, trigons are restricted to the octahedral crystal face and may occasionally form parallel rows that follow the orientation of plastic deformation lines (often called "grain lines" in the trade, caused by dislocation of carbon atoms along octahedral planes). In faceted diamonds, trigons are usually removed by polishing but are occasionally preserved on the girdle. Conversely, trigons reported within internal diamond etch channels are extremely rare (Lu et al., 2001). The occurrence of trigons within a subsurface channel indicates etching along the octahedral crystal face of this diamond.

Mei Yan Lai and Matthew Hardman

Figure 5. An irregular-shaped opening on the girdle where fluids/melts permeated through the diamond and formed the internal etch channels. Field of view 1.26 mm.

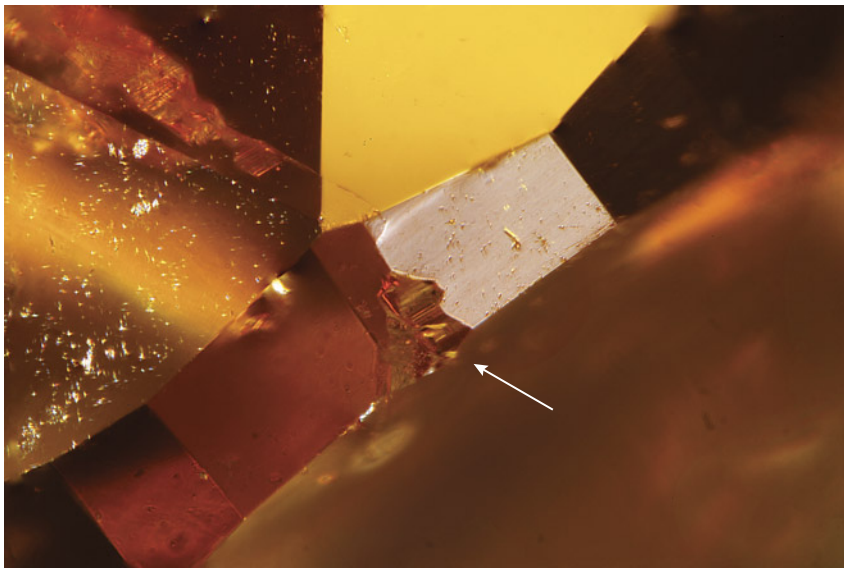

An Extraordinarily Large Cat's-Eye EMERALD

Emerald in cabochon form sometimes displays a chatoyant effect, and comparatively large cat's-eye emeralds are highly sought after. GIA's Tokyo labo-

Figure 7. An unusually large cat's-eye emerald weighing approximately 126 ct.

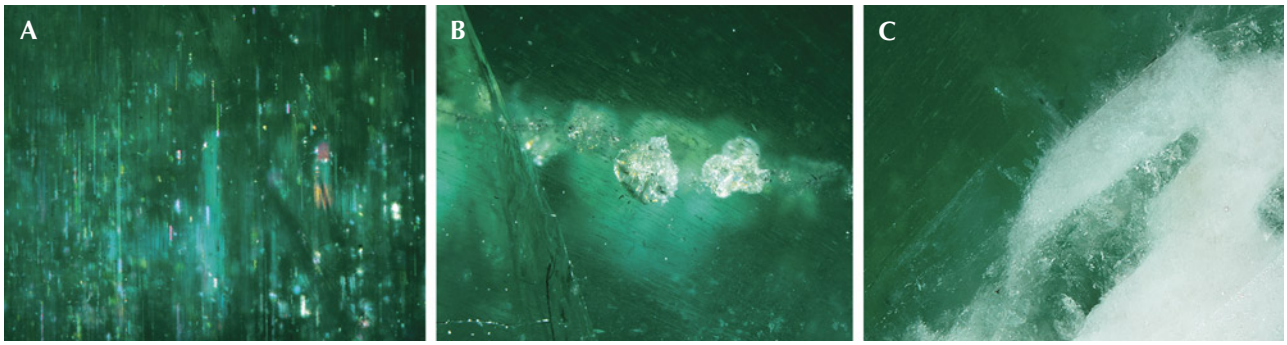

Figure 8. Inclusions observed in the large cat's-eye emerald. A: Rain-like inclusions; field of view 2.18 mm. B: Unknown whitish granular flake-like inclusions; field of view 5.70 mm. C: Aggregates of tiny whitish feldspar crystals confirmed by Raman spectroscopy; field of view 3.60 mm.

ratory recently examined an extraordinarily large semitransparent green cabochon measuring 31.3 × 26.2 × 20.9 mm and weighing approximately 126 ct (figure 7). The stone had a spot refractive index of 1.58 and showed specific chromium absorption lines in the red through a handheld spectroscope, and standard gemological properties identified it as emerald.

The emerald contained numerous reflective rain-like inclusions creating a chatoyant effect (figure 8A), whitish granular flake-like inclusions (figure 8B), and aggregates of tiny whitish crystals which were identified as feldspar by Raman spectroscopic analysis (figure 8C). The ultraviolet/visible/near-infrared absorption spectra showed two broad bands of Cr^{3+} at 430 and 600 nm, with a large Fe^{2+} band at around 850 nm and an Fe^{3+} broad band at 372 nm. Trace element chemical results using laser ablation–inductively coupled plasma–mass spectrometry showed that this emerald had a high iron concentration (2800–2930 ppmw) and medium potassium range (67.8–74.3 ppmw), characteristics similar to the published data of emeralds from the Belmont mine in Minas Gerais, Brazil (e.g., S. Saeseaw et al., "Geographic origin determination of emerald," Winter 2019 *G&G*, pp. 614–646). Inclusions observed in this emerald were also consistent with a Brazilian origin (again, see figure 8).

Brazil is a well-known source of large emerald crystals. One previous report (Summer 2015 Gem News International, pp. 200–201) described a 43 ct Brazilian cat's-eye emerald. The cat's-eye emerald examined here is notable for its size and transparency, and it is one of the largest examined by a GIA laboratory to date.

Makoto Miura

A "Cobalt Blue" GAHNOSPINEL

GIA's Bangkok laboratory recently examined an intense blue 1.01 ct transparent oval mixed cut (figure 9). Standard gemological testing revealed a refractive index of 1.742 and a hydrostatic specific gravity of 3.96. The stone was inert to long-wave and short-wave UV light. Microscopic observation revealed dense intersecting needles, iridescent thin films, particulate clouds, and flaky whitish inclusions. Laser ablation–inductively coupled plasma–mass spectrometry (LA-ICP-MS) was used to obtain oxide weight percentages (wt.% oxides) of aluminum, iron, magnesium, and zinc to calculate the chemical formula of the stone. It was determined to be $(Mg_{0.64}Fe^{2+}_{0.02}Zn_{0.34})Al_2O_4$. All of these properties were consistent with gahnospinel, which is a zinc-rich variety of the spinel group. Its chemical properties result from zinc substituting for magnesium in a solid solution series with end members gahnite ($ZnAl_2O_4$) and spinel ($MgAl_2O_4$).

Figure 9. This 1.01 ct gahnospinel had an intense "cobalt blue" color.

Interestingly, gahnospinel is usually found with a more muted dark blue to dark greenish blue color, but this intense blue specimen contained cobalt as the primary coloring agent, similar to "cobalt blue" gem spinel. Ultraviolet/visible (UV-Vis) spectroscopy showed significant amounts of absorption attributable to cobalt at approximately 550, 593, and 622 nm (figure 10), with additional contribution from iron at approximately 456, 550, and 593 nm (G.B. Andreozzi et al., "Color mechanism in spinel: A multi-analytical investigation of natural crystals with a wide range of coloration," *Physics and Chemistry of Minerals*, Vol. 46, 2019, pp. 343–360; V. D'Ippolito et al., "Color mechanism in spinel: Cobalt and iron interplay for the blue color," *Physics and Chemistry of Minerals*, Vol. 42, 2015, pp. 431–439). The significant amount of cobalt (198–224 ppmw) from LA-ICP-MS data and the reddish Chelsea filter reaction provided strong evidence that the intense blue color was induced by cobalt. While blue cobalt spinel and gahnite have been previously reported (see J.E. Shigley and C.M.

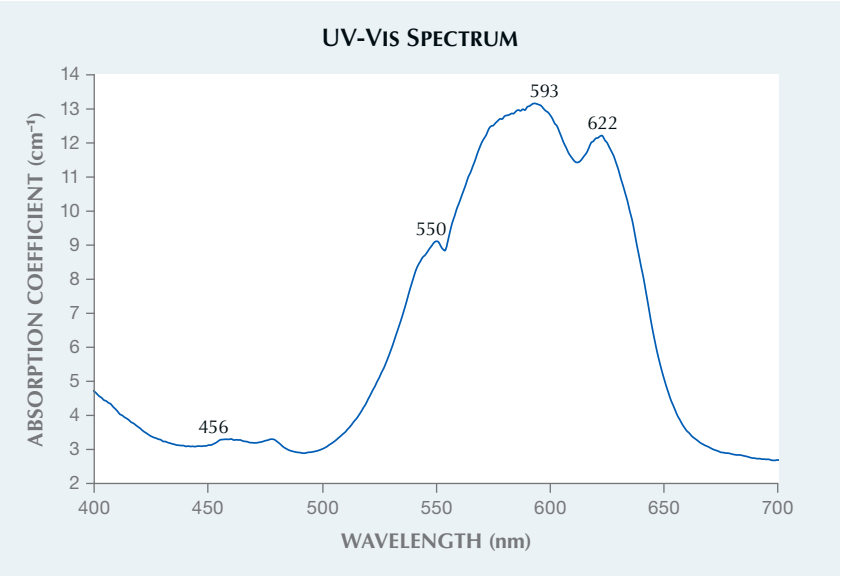

Figure 10. The UV-Vis spectrum of the gahnospinel showed a series of absorption bands at approximately 550, 593, and 622 due largely to Co^{2+} with additional minor contributions from Fe^{2+} and Fe^{3+} absorption bands at approximately 456, 550, and 593 nm.

Stockton, "'Cobalt-blue' gem spinels," Spring 1984 *G&G*, pp. 34–41; T. Stephan et al., "On the colour mechanism of blue gahnite from Nigeria," *Journal of Gems & Gemmology*, Vol. 38, No. 2, 2022, pp. 183–193), to our knowledge this is the first report of blue gahnospinel predominantly colored by cobalt.

Narint Jaisanit

PEARLS

Calcite Found on the Surface of a Saltwater "Nacreous" Pearl

The Hong Kong laboratory recently examined a loose pearl weighing 2.32 ct and measuring 8.45 × 7.27 × 5.36 mm (figure 11). Externally, the cream-colored pearl did not look out of the ordinary and exhibited a soft luster with a relatively clean surface. Examination through a binocular microscope revealed typical overlapping platelets, pits, and scratches. No coating, surface working, or other indications of treatment were observed (figure 12).

Figure 12. The pearl exhibited overlapping surface platelets typically found in nacreous pearls. Field of view 1.10 mm.

Real-time microradiography (RTX) revealed a distinct boundary with twin growth structures consisting of normal growth layers that followed the shape of the pearl (figure 13). No structural characteristics of any known type of cultured pearl were observed, so the pearl was identified as a natural pearl. Energy-dispersive X-ray fluorescence analysis showed high levels of strontium and no traces of

Figure 11. A cream-colored button-shaped loose pearl weighing 2.32 ct, submitted for identification.

Figure 13. RTX examination revealed a clear boundary running across the pearl as well as structures associated with natural formation.

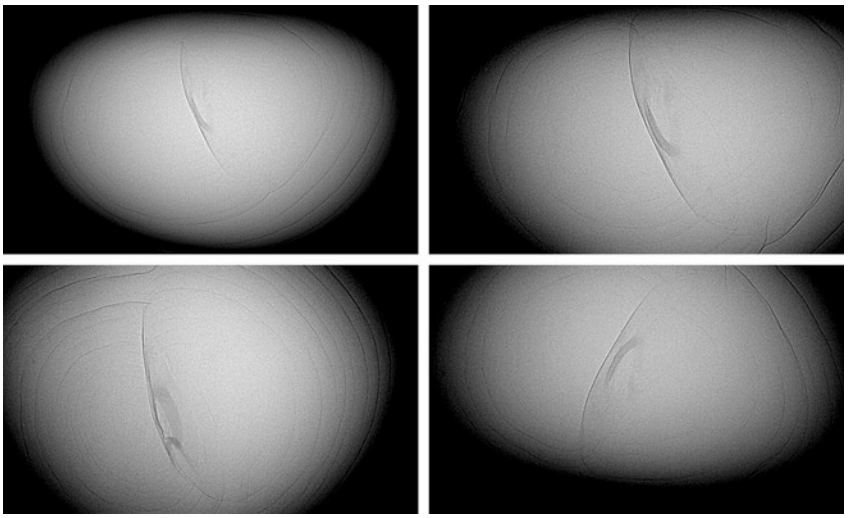

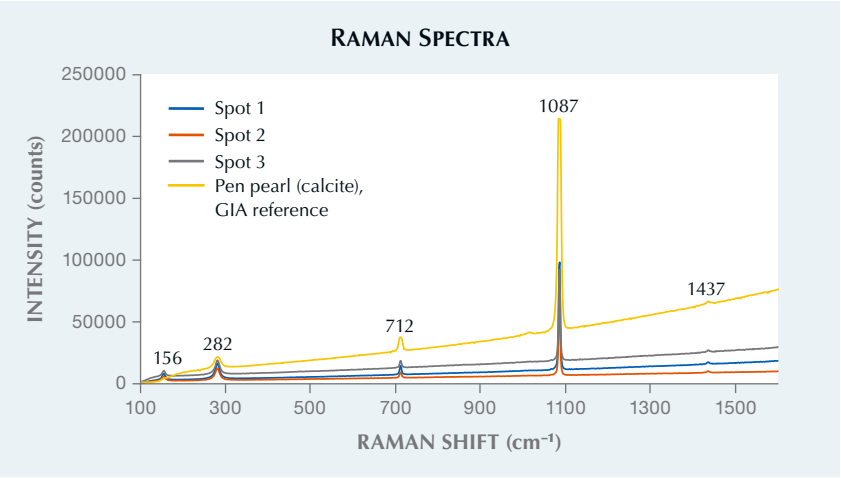

Figure 14. Raman spectra of three spots on the pearl's surface exhibit main peaks at 156, 282, 712, and 1087 cm^{-1} that are diagnostic of calcite.

manganese. This, together with its lack of visible fluorescence to X-ray luminescence, confirmed its saltwater origin.

Despite the typical saltwater nacreous pearl surface appearance, Raman analysis on three random spots with 514 nm laser excitation revealed that the pearl's platelet surface was composed of calcite rather than aragonite, with peaks at 156, 282, 712, 1087, and 1437 cm^{-1} (figure 14) (J. Urmos et al., "Characterization of some biogenic carbonates with Raman spectroscopy," *American Mineralogist*, Vol. 76, 1991, pp. 641–646).

Nacreous pearls are typically composed of small polygonal tablets of aragonite arranged in laminar layers (L. Addadi and S. Weiner, "A pavement of pearl," *Nature*, Vol. 389, 1997, pp. 912–915). Up until the examination of this specimen, Raman analysis on submitted pearls and research samples exhibiting overlapping platelet layers has always shown a mineral composition of aragonite. Calcite is usually found in the form of mosaic or cellular patterns on the surface of some types of pearls, or in the prismatic internal layers. This is the first time GIA has encountered a "nacreous-looking" pearl showing calcite when tested in different positions on its surface, which is unique and certainly worthy of note.

Cheryl Ying Wai Au

Two Black Non-Nacreous Bead Cultured Pearls from *Pinctada margaritifera*

The laboratory in Carlsbad recently received for identification two black pearls, one near-round and one button. The near-round pearl weighed 15.16 ct, while the button weighed 22.19 ct, with dimensions of 13.17 × 13.02 mm and 14.81 × 14.52 mm, respectively. Both displayed a similar vitreous luster and a non-nacreous surface appearance (figure 15). The button-shaped pearl also exhibited a nacreous surface on a small circled area at the base (figure 16). Microscopic examination using fiber-optic illumination revealed that the non-nacreous surface was composed of a mosaic or cellular pattern, resulting from the acicular nature of the individual calcite crystals. Some fine surface lines were also present in random directions across the cellular structures (figure 17). These cellular structures resembled those commonly observed on pen pearls from the Pinnidae family (N. Sturman et al., "Observations on pearls reportedly from the Pinnidae family (pen pearls)," Fall 2014 *G&G*, pp. 202–215).

A Raman spectrometer with 514 nm argon-ion laser excitation was used to examine the surface composition. The non-nacreous surfaces of both pearls showed a calcite spectrum with peaks at 712 and 1085 cm^{-1}, and aragonite peaks at 705 and 1085 cm^{-1} were

Figure 15. Left: Two black pearls, a 15.16 ct near-round and a 22.19 ct button, shown on the nacreous interior surface of a Pinctada margaritifera *shell. Right: The pearls both had a similar vitreous luster and a non-nacreous surface.*

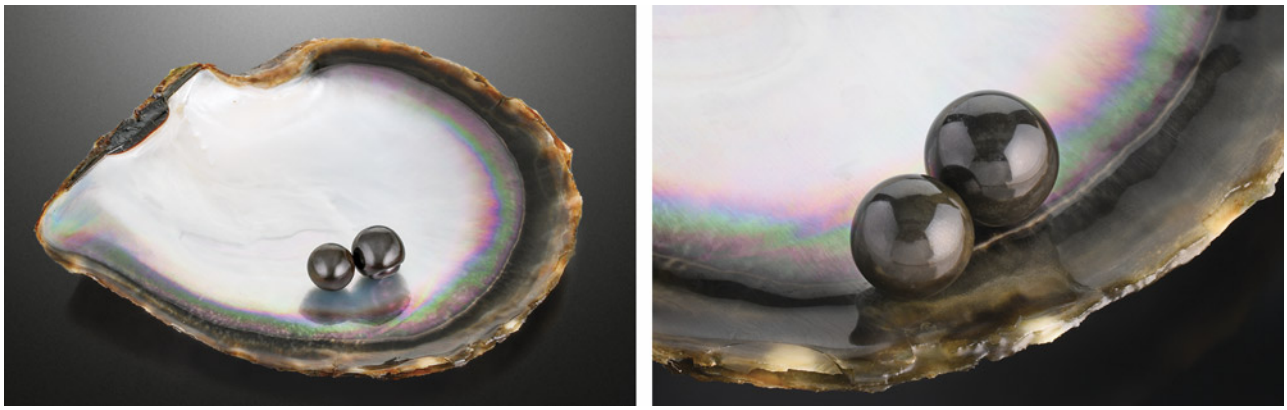

Figure 16. The button-shaped pearl displayed two different surface appearances. The main body was composed of a non-nacreous surface with calcite cellular structure, while the circled area at the base of the pearl had a nacreous surface with an aragonite platelet structure. Field of view 16.24 mm.

Figure 17. The non-nacreous surface of both pearls exhibited a similar cellular structure that could be viewed under high magnification using fiber-optic illumination. Some fine surface lines were present in random directions across the cellular structures. Field of view 1.59 mm.

recorded on the nacreous surface at the circular base of the button-shaped pearl. Energy-dispersive X-ray fluorescence chemical analysis showed low levels of manganese and high strontium content, confirming the pearls formed in a saltwater environment.

The large size, black bodycolor, and cellular structure of the pearls looked similar to the unusual non-nacreous natural pearls reportedly from *Pteria* species (S. Karampelas and H. Abdulla, "Black non-nacreous natural pearls from *Pteria* sp.," *Journal of Gemmology*, Vol. 35, No. 7, 2017, pp. 590–592) and a bead cultured (BC) pen pearl (Winter 2014 GNI, pp. 305–306) previously reported. Under long-wave ultraviolet radiation (365 nm), the pearls exhibited very weak yellow fluorescence that differed from the strong orangy red fluorescence observed in non-nacreous *Pteria* pearls. Real-time microradiography (RTX) revealed a round bead nucleus in the center of both pearls, indicating BC pearl origin (figure 18) similar to the previously reported BC pen pearl. Nevertheless, the ultraviolet/visible reflectance spectrum collected on the button pearl's nacreous surface showed a typical reflectance feature at 700 nm, a key mollusk identification feature attributed to *Pinctada margaritifera* pearls (K. Wada, "Spectral characteristics of pearls," *Gemological Society of Japan*, Vol. 10, No. 4, 1983, pp. 3–11, in Japanese). The reflectance features at 405 and 495 nm normally observed in naturally colored gray to black nacre of *P. margaritifera* shells were also present. Combining the cellular surface structures, BC origin, saltwater environment, and spectroscopic characteristics, we were able to conclude that both were non-nacreous BC pearls from the *P. margaritifera* mollusk.

All pearls are formed from calcium carbonate ($CaCO_3$) polymorphs such as aragonite and calcite together with organic substances as well as water. The most common form of $CaCO_3$ in pearls is a layered structure of aragonite platelets. This structure is the reason pearls display a nacreous surface and pearly luster. A non-nacreous surface indicates a pearl that formed from $CaCO_3$ but not with an aragonite platelet microstructure. Conch and Melo pearls are non-nacreous pearls that possess an aragonite fibrous or lamellar structure that display flame-like surface patterns. Scallop pearls are non-nacreous pearls made of calcite in a honeycomb patchwork of cells. Pen pearls mentioned previously are

Figure 18. RTX imaging revealed a round bead nucleus in the center of each pearl, indicating the pearls were bead cultured.

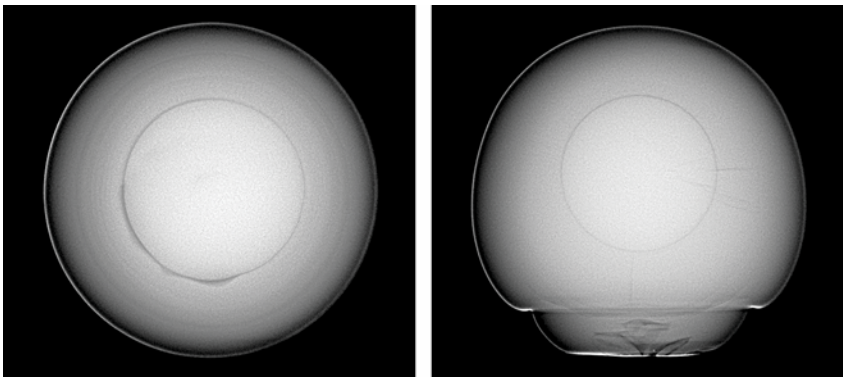

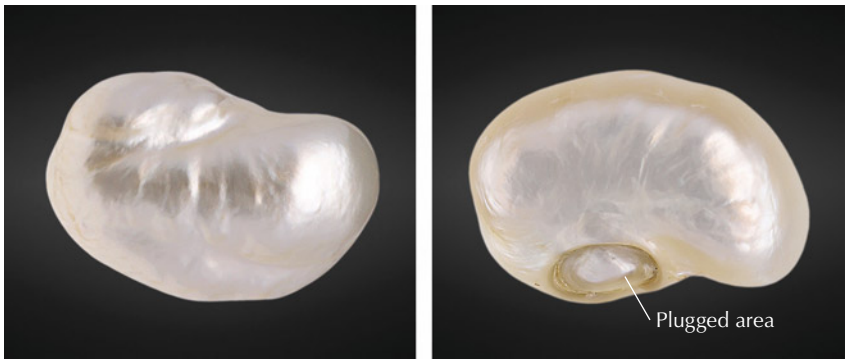

Figure 19. The 169.05 ct filled pearl, viewed from its face (left) and base (right). Note the indented feature on the base through which the filler material was inserted prior to plugging.

another type of calcite pearls with a cellular structure.

These two special occurrences are the first non-nacreous BC pearls from *P. margaritifera* identified by GIA. Cultured pearls from this mollusk, both BC and non-bead cultured, typically display a nacreous surface and are often referred to as "Tahitian" pearls in the market. Genetics is probably the most important factor influencing the biomineralization of a pearl, yet many other factors can be involved such as water environment and health of the mollusk. Organic substances also play an important role in the biomineralization process (C. Jin and J. Li, "The molecular mechanism of pearl biomineralization," *Annals of Aquaculture and Research*, Vol. 4, No. 1, 2017, p. 1032). In nature, many living organisms elaborately control the formation of biominerals for specialized functions such as mechanical support, protection, and mineral storage. Some mollusk species may produce different structures under certain circumstances.

Forozan Zandi, Artitaya Homkrajae, and Stephanie Shaw

A Partially Hollow Natural Blister Pearl Filled with Foreign Materials

Over the centuries, India has maintained its reputation as a natural pearl trading center. Since the launch of GIA's pearl identification service in Mumbai in May 2022, the laboratory has received a variety of interesting items for identification. One that stood out owing to its size and internal structure was a unique partially hollow natural blister pearl with unidentified fillers (figure 19).

The very large baroque white pearl weighed 169.05 ct (33.81 g) and measured 43.12 × 28.83 × 19.26 mm. However, on initial examination, its "heft" (perceived weight compared to its actual weight in comparison to its size) felt heavier than it should have. While the pearl's face-up side exhibited minor surface blemishes and good nacre condition (figure 20A), its base showed a deep oval indentation that looked a bit suspect to the unaided eye and needed further detailed examination. Under 40× magnification, the area revealed a distinct boundary with remnants of a transparent adhesive around it (figure 20B). Evidence of heavy working and polishing on and around the base was also clearly visible (figure 20, C and D).

Many loose nacreous baroque or semi-baroque pearls of this size are hollow to some degree, and most turn out to be blister pearls that were attached to the shell and removed at some point ("An unusual pearl," *GIA Research News*, March 31, 2009) or were shell blisters. In order to ensure the durability of these hollow pearls, and sometimes to add weight and increase their perceived value, they are filled with various materials such as metals, resins, waxes, shell, and other pearls (Fall 2013 Lab Notes, pp. 172–

Figure 20. A: The pearl's face showed minor surface blemishes; field of view 8.00 mm. B: The plugged area (boundary indicated by arrows) on the base with remnants of an adhesive around the oval opening; field of view 1.60 mm. C and D: Smoothed nacre layers provide evidence of heavy working and polishing on the base; field of view 3.00 mm.

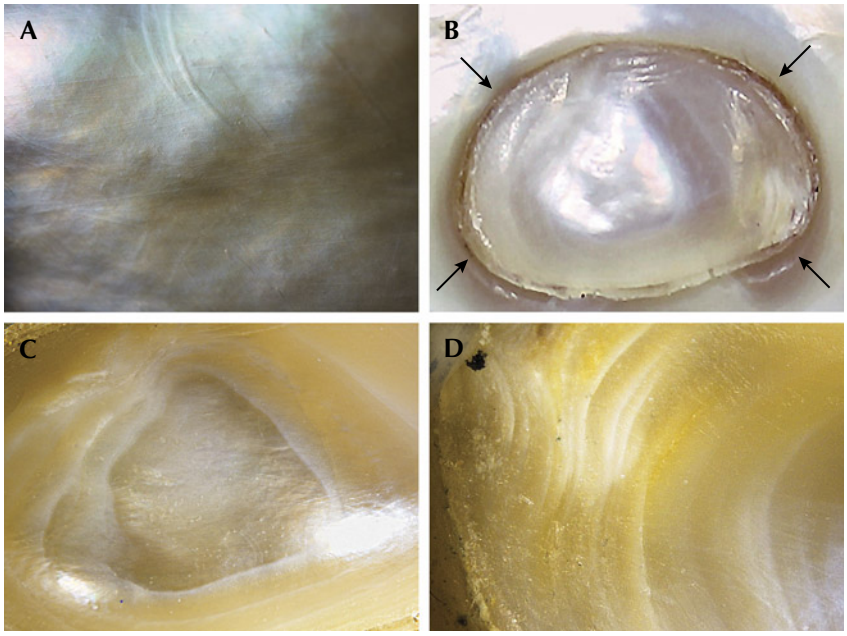

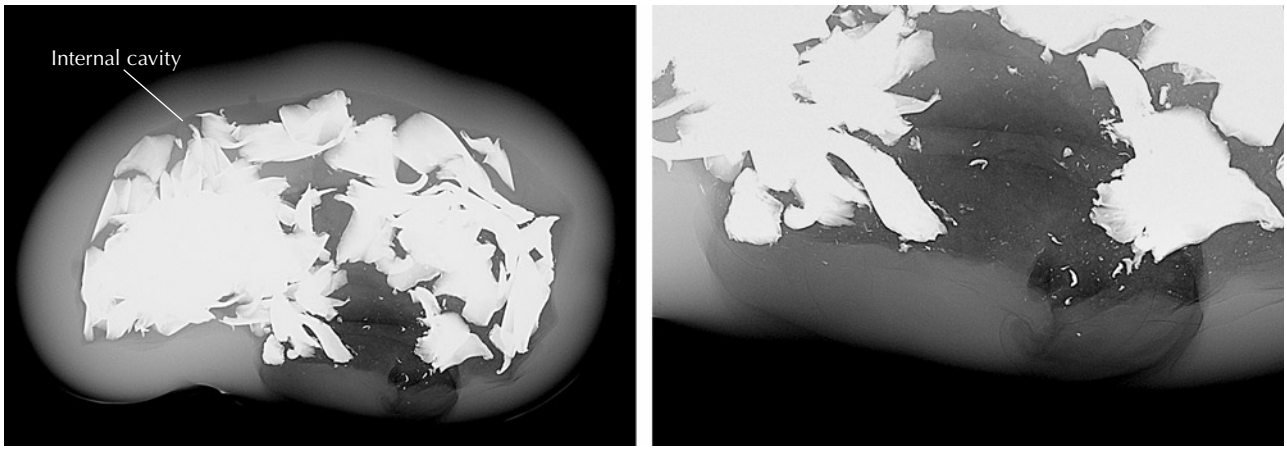

Figure 21. Opaque (white) areas indicate that metal pieces were placed within the pearl's large internal cavity (left). Natural growth arcs and a small darker organic-rich area are visible at the pearl's base (right).

173) and fashioned to improve their external appearance. Although the initial examination indicated that this pearl was likely filled with foreign materials, further analysis was required.

Real-time microradiography revealed a large organic void/cavity filled with a radiopaque white material, probably small metal fragments or metal shavings (figure 21; see also Summer 2019 Lab Notes, pp. 251–254). Areas of greater radio-transparency suggested that some type of bonding or stabilizing material, possibly adhesive, may have been used to hold the foreign pieces in place, and there also appeared to be one other type of radiolucent material within the cavity. The pearl was examined in several directions in order to further analyze the internal structure and fillings. The outline of the void was smooth and blended with the external shape of the pearl. The outer nacre layers revealed fine growth arcs and a small organic-rich area was visible at the base, both of which aligned more with the growth features of a natural pearl. It was clear that this was originally a blister pearl or shell blister that had been cut from a shell, and that the indented area, which was the opening on the base of the pearl, was the point of attachment that was subsequently plugged. X-ray fluorescence proved that the pearl formed in a saltwater environment since most of its surface appeared inert and only a small area at the base displayed a very light greenish yellow reaction uncharacteristic of a freshwater environment.

Energy-dispersive X-ray fluorescence spectrometry on two areas (face and base) showed low or below detection levels of manganese and higher strontium levels, above 1000 ppm, both characteristic of a saltwater environment. The higher strontium levels coupled with the large size indicated that the mollusk from which the pearl originated was *Pinctada maxima*.

Raman analysis using a 514 nm laser excitation on two spots (face and base) of the surface produced high fluorescence due to the pearl's light color and showed a doublet at 702 and 705 cm^{-1} as well as a peak at 1085 cm^{-1} indicative of aragonite. The photoluminescence spectra also displayed high fluorescence together with the aragonite peaks, as observed via Raman, typical of most nacreous pearls. Ultraviolet/visible/near-infrared spectra within the 220–850 nm range collected from the face and base were as expected for white to light cream-colored pearls and showed a predominantly high reflectance. The presence of a prominent 280 nm absorption feature coupled with moderate yellow reaction under long-wave UV excitation indicated that bleaching had most likely not been carried out.

After conducting a full analysis, GIA concluded that this sample most likely formed as a hollow natural blister pearl attached to its shell host. At some point, it was removed and the attachment area left an opening into the pearl. It was eventually worked and filled with foreign fillers (metal shavings/pieces and possibly some other materials) to improve its durability and make it suitable for setting; without the filling, it would not be usable in jewelry. The size, spectral characteristics, and chemistry were also consistent with a *Pinctada maxima* host mollusk.

Roxane Bhot Jain, Abeer Alalawi, Nicholas Sturman, and Chunhui Zhou

Large Faceted Pallasitic PERIDOT

Peridot, the green gem variety of the mineral olivine, is a relatively common gemstone known for forming as irregular nodules in lava flows or as large crystals within pockets of solidified rock throughout many areas of the world. Rarely, this stone can also be sourced from stony iron meteorites that have survived their flaming passage through Earth's atmosphere. These peridot-containing meteorites are known as pallasite, and the gems they contain are known as pallasitic peridot. Due to the extreme conditions endured by extraterrestrial stones, examples of faceted pallasitic peridot usually weigh less than half a carat (A.H. Shen et al., "Identification of extraterrestrial peridot by trace elements," Fall 2011 *G&G*, pp. 208–213). A recent submission to the

TABLE 1. Concentrations of trace elements (in ppmw) in a pallasitic peridot.

Element	Faceted stone	Extraterrestrial range[a]	Terrestrial range[a]
V	12.00	9.18–23.4	0.11–4.46
Li	0.48	0.21–0.96	1.10–14.5
Ni	17.3	8.53–112	1770–4070
Mn	2090	1920–2490	772–1410
Zn	6.59	5.20–9.98	9.04–67.4
Co	6.47	4.37–19.6	84.8–147

[a]*From A.H. Shen et al., "Identification of extraterrestrial peridot by trace elements," Fall 2011 G&G, pp. 208–213.*

Figure 22. The face-up view of a 2.32 ct faceted pallasitic peridot, the largest extraterrestrial peridot seen at GIA to date.

Carlsbad laboratory saw the largest client-submitted example to date at 2.32 ct (figure 22). The gem possessed characteristic inclusions such as thin, stacked red platelets (figure 23, left) and coarse, high-relief fingerprints (figure 23, right).

At GIA, extraterrestrial peridot is distinguished from the terrestrial variety by either energy-dispersive X-ray fluorescence or laser ablation–inductively coupled plasma–mass spectrometry (LA-ICP-MS) analysis of the trace elements vanadium, lithium, nickel, manganese, zinc, and cobalt (Shen et al., 2011). LA-ICP-MS analysis of these elements in the stone was diagnostic of pallasitic peridot when compared to published terrestrial and extraterrestrial data (Shen et al., 2011) (table 1).

Pallasite is named in honor of geologist Peter Simon Pallas, who first documented a stony iron meteorite with "rounded and elongated drops of a very brittle but hard, amber-yellow, transparent glass" discovered in Krasnoyarsk, Siberia, in 1749. At the time, suggestion of an extraterrestrial origin was daring. However, this theory gained support, and by 1794 additional scientific publications accepted the idea (J. Sinkankas et al., "Peridot as an interplanetary gemstone," Spring 1992 *G&G*, pp. 43–51). Today, pallasite is believed to have formed within asteroids containing an iron-nickel core and a silicate mantle (R.T. Dodd, *Meteorites: A Petrologic-Chemical Synthesis*, Cambridge University Press, Cambridge, UK, 1981, 368 pp.).

Britni LeCroy

PHOTO CREDITS
Shunsuke Nagai—1, 7; Yuxiao Li—2; Matthew Hardman—3–5; Mei Yan Lai—6; Makoto Miura—8; Lhapsin Nillapat—9; Tony Leung—11; Nick Chan—12; Cheryl Ying Wai Au—13; Annie Haynes—15; Artitaya Homkrajae—16, 17; Stephanie Shaw—18; Gaurav Bera—19; Nishka Vaz—20; Jayesh Surve—21; Diego Sanchez—22; Britni LeCroy—23

Figure 23. Left: Planar, brownish red thin films are a distinctive inclusion in pallasitic peridot; field of view 1.26 mm. Right: Coarse fingerprints are a common inclusion in both terrestrial and extraterrestrial peridot; field of view 1.99 mm.